ACS APPLIED MATERIALS & INTERFACES

Research Article

www.acsami.org

New Chemical Route for the Synthesis of β-$Na_{0.33}V_2O_5$ and Its Fully Reversible Li Intercalation

Jae-Kwang Kim,[†] B. Senthilkumar,[†] Sun Hye Sahgong,[†] Jung-Hyun Kim,*[,‡] Miaofang Chi,[§] and Youngsik Kim*[,†]

[†]School of Energy and Chemical Engineering, Ulsan National Institute of Science and Technology, Ulsan, 689-798, South Korea

[‡]Chemical and Materials Systems Laboratory, General Motors Global Research & Development Center, Warren, Michigan 48090-9055, United States

[§]Materials Science and Technology Division, Oak Ridge National Laboratory, Oak Ridge, Tennessee 37831-6064, United States

Supporting Information

ABSTRACT: To obtain good electrochemical performance and thermal stability of rechargeable batteries, various cathode materials have been explored including $NaVS_2$, β-$Na_{0.33}V_2O_5$, and $Li_xV_2O_5$. In particular, $Li_xV_2O_5$ has attracted attention as a cathode material in Li-ion batteries owing to its large theoretical capacity, but its stable electrochemical cycling (i.e., reversibility) still remains as a challenge and strongly depends on its synthesis methods. In this study, we prepared the $Li_xV_2O_5$ from electrochemical ion exchange of β-$Na_{0.33}V_2O_5$, which is obtained by chemical conversion of $NaVS_2$ in air at high temperatures. Crystal structure and particle morphology of β-$Na_{0.33}V_2O_5$ are characterized by using X-ray diffraction, scanning electron microscopy, and transmission electron microscopy techniques. Energy-dispersive X-ray spectroscopy and X-ray photoelectron spectroscopy, in combination with electrochemical data, suggest that Na ions are extracted from β-$Na_{0.33}V_2O_5$ without irreversible structural collapse and replaced with Li ions during the following intercalation (i.e., charging) process. The thus obtained $Li_xV_2O_5$ delivers a high discharge capacity of 295 mAh g^{-1}, which corresponds to $x = 2$, with crystal structural stability in the voltage range of 1.5−4.0 V versus Li, as evidenced by its good cycling performance and high Coulombic efficiency (under 0.1 mA cm^{-2}) at room temperature. Furthermore, the ion-exchanged $Li_xV_2O_5$ from β-$Na_{0.33}V_2O_5$ shows stable electrochemical behavior without structural collapse, even at a case of deep discharge to 1.5 V versus Li.

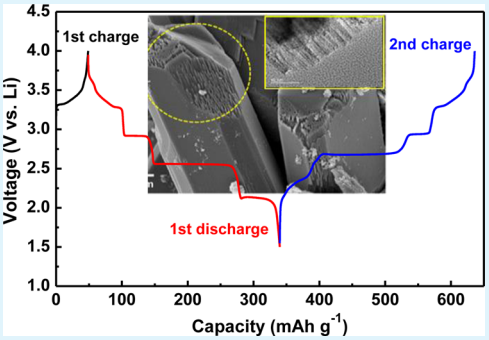

KEYWORDS: *β-$Na_{0.33}V_2O_5$, chemical switch, vanadium sulfides, vanadium oxides, structural collapse, high capacity cathode*

1. INTRODUCTION

Vanadium pentoxide, V_2O_5, was one of the first oxides to be studied for use as a cathode in lithium-ion batteries because its structure consists of VO_5 square pyramid layers with an open Li intercalation site between the layers. The open structure could combine with the wide range of oxidation states for vanadium, which allows for a high theoretical specific capacity of 442 mA h g^{-1} for $Li_xV_2O_5$ at $x = 3$. In addition, vanadium is abundant in the crust of Earth, guaranteeing the availability and low cost of V_2O_5.[1−3] However, vanadium pentoxide has suffered from poor specific capacity and cyclability because of its low diffusion coefficient of lithium ions and irreversible structural change when Li insertion is greater than $x = 1$.[4−6] Great effort has been made over the last 20 years to improve the phase reversibility of $Li_xV_2O_5$ (e.g., $0 \leq x \leq 2$) by influencing the compound's structure and surface defects as well as its particle size and morphology, the latter of which has been created by various synthesis methods and post-treatment conditions.[7−12]

One of the trials found that a more stable and rigid 3D framework structure with a tunnel was achieved by doping with metallic species (such as Na) into the V_2O_5, producing β-$Na_{0.33}V_2O_5$.[13,14] β-$Na_{0.33}V_2O_5$ contains three different open intercalation sites (M1−M3) in its 3D tunnel structure where Li can be reversibly intercalated at the range of $0.0 \leq x \leq 1.66$. Additionally, the phase transformations observed in $Li_x\beta$-$Na_{0.33}V_2O_5$ are reversible during cycling, which provides a specific capacity up to 234 mA h g^{-1} at $x = 1.66$. Many types of synthesis methods for β-$Na_{0.33}V_2O_5$, which include solid-state reaction,[15,16] flux method,[17] sol−gel method,[18−20] and hydrothermal method,[14,21−23] have been attempted to enhance its electrochemical performances. A recent report, based on hydrothermal-synthesized β-$Na_{0.33}V_2O_5$ shows high capacity of 339 mA h g^{-1} and structure stability at depth discharge of 1.5 V.[23]

Herein, we primarily reported the chemical switching from $NaVS_2$ to β-$Na_{0.33}V_2O_5$ and investigated the structure and phase evolution underlying the lithiation/delithiation process of β-$Na_{0.33}V_2O_5$, which is critical for improving electrochemical

Received: February 9, 2015
Accepted: March 13, 2015
Published: March 13, 2015

DOI: 10.1021/acsami.5b01260
ACS Appl. Mater. Interfaces 2015, 7, 7025−7032

properties. In this work, β-$Na_{0.33}V_2O_5$ was synthesized via a new chemical route involving a chemical switch of the $NaVS_2$ heat-treated at 600 °C in air atmosphere for the first time. The Na ions of β-$Na_{0.33}V_2O_5$ were extracted from the compound's structure, and $Li_xV_2O_5$ was prepared by electrochemical ion exchange. The subsequent intercalation of Li ions into $Li_xV_2O_5$ was observed with $0.0 \leq x \leq 2.0$ without irreversible phase change. To the best of our knowledge, Na extraction from $Na_{0.33}V_2O_5$ has not been reported elsewhere, and the more inserted lithium ions ($x = 2$) than 1.66 Li into $Na_{0.33}V_2O_5$, the higher the capacity achieved, which is beneficial to obtaining high energy density.

2. EXPERIMENTAL SECTION

2.1. Preparation of the Samples. To prepare $NaVS_2$, appropriate amounts of Na_2S (Sigma, 99%), vanadium (Alfa, 99.5%), and sulfur (Sigma, 99.99%) were mixed together and placed in a carbon-coated quartz tube inside an Ar glovebox. Then, the quartz tube was sealed under vacuum. The sealed tube was slowly heated over 20 h to 700 °C, next kept for 40 h at 700 °C, and then slowly cooled over 5 h to 250 °C, followed by quenching the tube in air. While inside an Ar glovebox, the samples were removed from the tubes and then thoroughly ground and pelletized. Because $NaVS_2$ is sensitive to moisture, it was always handled under an Ar atmosphere.

To prepare the vanadium oxides, the $NaVS_2$ powders were loaded into an Al_2O_3 crucible and then placed into the furnace in atmospheric air. The powders were slowly heated over 5 h to reach 400, 500, and 600 °C and held for 10 h at each of these temperatures, followed by allowing them to naturally cool to room temperature.

2.2. Structural Analysis. The powder X-ray diffraction (XRD) data was collected using the Bruker D8 Advanced diffractometer equipped with Cu Kα radiation and a diffractometer monochromator that was operated at 40 kV and 40 mA. The samples were finely ground and placed in the sample holder of the diffractometer. Data for Rietveld structure refinement was obtained in the 2θ range = 15−120°, with a 0.02° step interval and a 10 s step time. The sample was rotated at 30 rpm during data collection to minimize any preferred orientation and statistical errors in calculation. The crystal structure was refined in the space group $C2/m$ using the program GSAS. The morphology of the sample particles was analyzed by scanning electron microscopy (SEM), and the particle surfaces were further characterized using transmission electron microscopy (TEM). The TEM microscope was an aberration-corrected JEOL JEM-2100F operated at 200 kV. Samples were made suitable for TEM observation by grinding the heat-treated material into fine powders and dusting them onto lacy-carbon-coated copper TEM grids.

2.3. Electrochemical Analysis. The electrode and cell were prepared in an Ar glovebox. The electrodes were fabricated from a 70:20:10 (wt %) mixture of active material, acetylene black as current conductor, and poly(tetrafluoroethylene) as binder. The mass, diameter, and thickness of a typical electrode were 10 mg, 7 mm, and 0.06 mm, respectively. The electrochemical cells were prepared with standard 2016 coin cell hardware, using Li metal foil as both the counter and reference electrodes. The electrolyte used for analysis was 1 M $LiPF_6$ in 1:1 EC/DEC. The sealed cells were taken out of the Ar glovebox and placed in a battery testing system. Electrochemical performance tests were carried out using an automatic galvanostatic charge−discharge unit, WBCS 3000 battery cycler, between 1.5 and 4.0 V at room temperature. The experiments were carried out at 0.1 mA cm^{-2} current density. The cells were then aged for 5 h before the first discharge (or charge) to ensure full absorption of the electrolyte into the electrode.

3. RESULTS AND DISCUSSIONS

3.1. Chemical and Structural Characterizations. This study takes a unique approach to synthesizing a high-quality sodium vanadium bronze, β-$Na_{0.33}V_2O_5$, with enhanced crystallinity via the chemical switch of $NaVS_2$ heat-treated in air. The pristine $NaVS_2$ sample has an hexagonal structure, consisting of hexagonal close-packed sulfur with V and Na atoms in alternate octahedral-site (001) planes forming a layered structure.[2,3] The XRD patterns of the $NaVS_2$ sample (Figure 1) matched well to those reported in the literature, and such details of their crystal structures were discussed.[2,3]

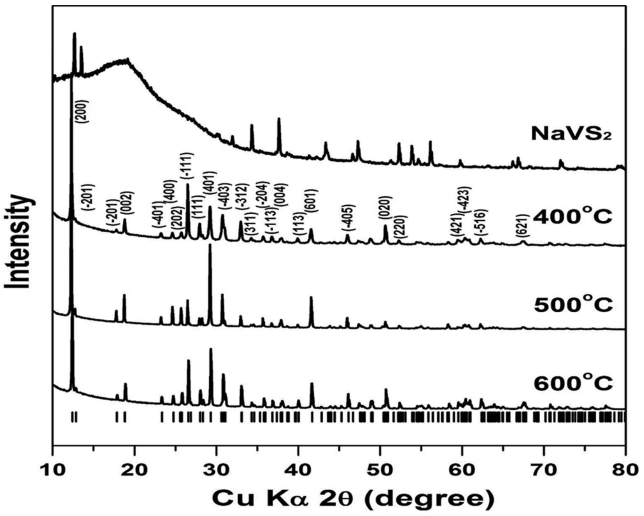

Figure 1. Powder XRD patterns for $NaVS_2$ and its samples that were heat-treated for 10 h under air at different temperatures, with crystal structure of layered $NaVS_2$ and 3D framework β-$Na_{0.33}V_2O_5$.

When the $NaVS_2$ sample was exposed to atmospheric air and heated at a high temperature of 600 °C for 10 h, the initial sulfide phase became the mixtures of Na_2SO_4 and β-$Na_{0.33}V_2O_5$ identified by the XRD (see Figure S1). Na_2SO_4 was produced as a result of $NaVS_2$ decomposition during heat-treatment in air and could be eliminated by washing with water as shown in Figure S1. Therefore, heat-treated samples were washed with water to remove the Na_2SO_4 phase before further analyses. Figure 1 shows XRD patterns of the washed samples. The XRD data from all three samples (400, 500, and 600 °C) can be indexed on the basis of the β-$Na_{0.33}V_2O_5$ phase with a monoclinic symmetry (space group: $C2/m$), which has a 3D tunneling structure along the [010] direction.[18−20] The results of Rietveld refinement obtained from a least-squares fitting of the XRD data are summarized in Table S1. These results indicate that the chemical and phase transformations of $NaVS_2$ toward β-$Na_{0.33}V_2O_5$ appeared by air oxidation of $NaVS_2$ at temperatures in the range of 400−600 °C. However, the 600 °C calcined sample showed highly crystallinity with a formation of high-temperature monoclinic β-$Na_{0.33}V_2O_5$ phase. It also presented typical electrochemical voltage profiles (see Figure S2) of the β-$Na_{0.33}V_2O_5$ phase, which agrees well with literature data.[18,23] Therefore, further characterizations were performed for the 600 °C calcined sample.

Figure 2 shows the crystal structures determined by the Rietveld refinement for β-$Na_{0.33}V_2O_5$ (Figure 2a). Sodium vanadium bronze, β-$Na_{0.33}V_2O_5$ has a monoclinic structure, the same as LiV_2O_5 (Joint Committee on Powder Diffraction Standards, JCPDS, no. 73-1670). However, the radius of a sodium ion is much larger than that of a lithium ion. Thus, β-$Na_{0.33}V_2O_5$ possesses a larger interlayer distance ($Na_{0.33}V_2O_5$, 7.06 Å; $Li_xV_2O_5$, 6.36 Å), a higher lithium diffusion coefficient as well as reduced interaction between the interlayer cations.[24]

DOI: 10.1021/acsami.5b01260
ACS Appl. Mater. Interfaces 2015, 7, 7025−7032

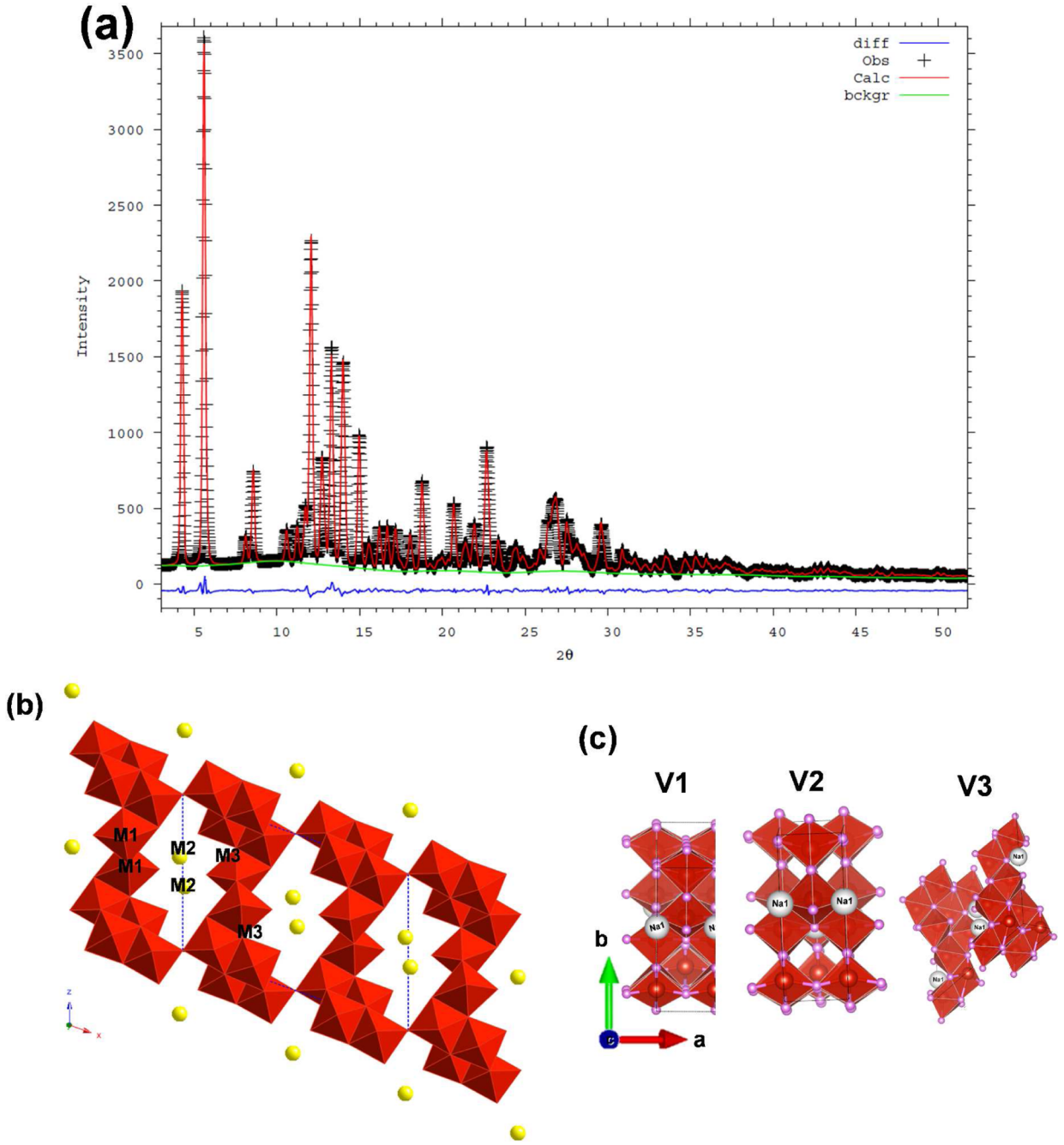

Figure 2. (a) XRD pattern and Rietveld refined result of β-$Na_{0.33}V_2O_5$. (b) Projection of the crystal structure of β-$Na_{0.33}V_2O_5$ on the $a-c$ plane and possible positions (M1−M3) of the inserted cations. (c) Structural subunits of β-Na0.33 V2O5: zigzag chains of edge-sharing (V1)O6 octahedra; two-leg ladders of corner-sharing (V2)O6 octahedra; zigzag chains of (V3)O5 polyhedra.

Table 1. Structural Parameters of Powder β-$Na_{0.33}V_2O_5$ Samples

heating temp. (°C)	phase	space group	a (Å)	b (Å)	c (Å)	β (deg.)	unit cell volume (Å^3)
400	β-$Na_{0.33}V_2O_5$	$C2/m$	10.072	3.609	15.381	109.552	526.80
500	β-$Na_{0.33}V_2O_5$	$C2/m$	10.068	3.608	15.343	109.378	525.77
600	β-$Na_{0.33}V_2O_5$	$C2/m$	10.068	3.607	15.387	109.556	526.59

Moreover, the volume change of $Na_{0.33}V_2O_5$ during the Li-ion insertion/extraction processes is smaller. Therefore, β-$Na_{0.33}V_2O_5$ has the potential to show improved cyclic performance and rate capability.

Although β-$Na_{0.33}V_2O_5$ prepared by our chemical switch method is the same in structure as monoclinic β-$Na_{0.33}V_2O_5$ ($C2/m$ space group), the crystal density is higher, the lattice parameter of a axis is shorter, and the c axis is longer (Table 1) than the published data for typical β-$Na_{0.33}V_2O_5$. The difference can be found from (V3)O6 octahedra (atomic labels and their corresponding locations are described in Table S1); the (V3)O6 octahedra of our chemically switched β-$Na_{0.33}V_2O_5$

DOI: 10.1021/acsami.5b01260
ACS Appl. Mater. Interfaces 2015, 7, 7025−7032

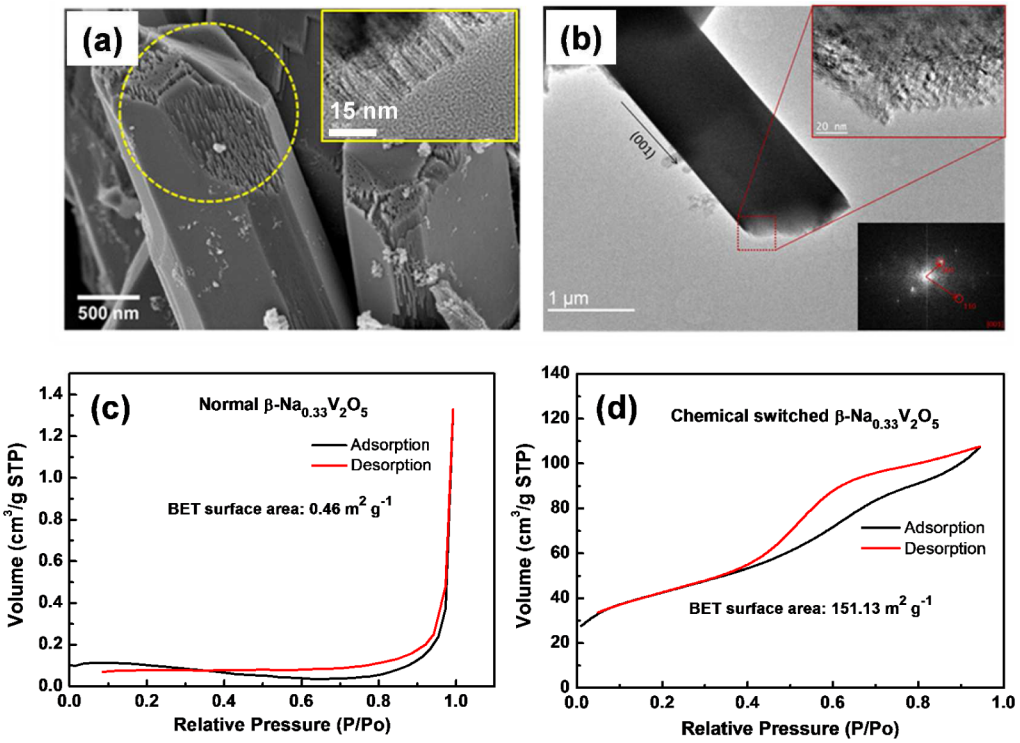

Figure 3. (a) Crystal defects were observed on the surface of the rod-shaped crystals, circled in yellow, where the high-resolution SEM image was taken. (b) TEM image of a rod-shaped particle of β-$Na_{0.33}V_2O_5$, which reveals that the longitudinal surface of the particle is (001) and that a considerable amount of stacking faults exist parallel to this face, SAED dot pattern indexed with (001) and (110) planes. (c and d) Nitrogen sorption isotherms and mesopore size distributions in the general β-$Na_{0.33}V_2O_5$ and the chemically switched β-$Na_{0.33}V_2O_5$, respectively.

grows in the z direction, whereas reported data from typical β-$Na_{0.33}V_2O_5$ showed its growth toward the (y,z) direction (Figure 2b).[24] We speculate that this octahedral growth in the z direction can provide a pillar effect and may be beneficial to maintain stable electrochemical performance without structural collapse during lithiation down to 1.5 V, which is similar to that recently reported on mesoporous β-$Na_{0.33}V_2O_5$.[23]

As shown in Figure 2b, β-$Na_{0.33}V_2O_5$ bronze crystallizes in a monoclinic tunnel-like structure (space group $C2/m$ with $Z = 6$ formula units per unit cell). In the crystal structure, a characteristic ladder-like V_2O_5 host framework is formed by edge/corner sharing of VO_6 octahedra and VO_5 square pyramids.[17,18] There are three structural units with three different sites for vanadium atoms: V_1 is coordinated with six oxygen forms, $V_1(O_6)$ octahedra, which build zigzag double-chain by sharing edges; $V_2(O_6)$ octahedra form a ladder chain by sharing corners; and V_3 sites have 5-fold square pyramidal coordination forms, $(V_3)O_5$ polyhedron (Figure 2c).[17] Vanadium-centered polyhedrons in one layer form zigzag double-chains that construct the 3D network along the b axis. The V_2O_5 host framework gives rise to unidirectional tunnel along the crystallographic b axis into which the Na ions are inserted.

Highly anisotropic quasi-1D conductivity of the tunnel is owed to the partial reduction of the V_2O_5 framework.[25] Na ions are located in four interstitial sites per unit cell along the b axis (M_1). The tunnel structure of β-$Na_{0.33}V_2O_5$ bronze has two additional tunnel sites for Li intercalation, four eight-coordinated sites (M_2), and four tetrahedral sites (M_3) per unit cell (Figure 2b).[23−25] Atomic positions and thermal factors are gathered in Table S1.

A high-magnification SEM image shows that β-$Na_{0.33}V_2O_5$ was well-crystallized and rod-shaped with a length of 7−15 μm and a width of 1−3 μm, as shown in Figure 3a. The 600 °C sample particles have surface defects in the shape of crystals around the edges of the particles, which exposes layers of grains (highlighted with a yellow dotted line). The high-resolution TEM image in Figure 3b also shows the layered grains along the crystal defects. The TEM image reveals that the longitudinal surface of the rod-shaped particle is parallel to (001) where a considerable amount of stacking faults exist at particle edges. It is plausible that the growth of the rod-shaped β-$Na_{0.33}V_2O_5$ crystals could be interfered with by coexisting Na_2SO_4 salt crystals at the edge (or surface) area during heat-treatment at 600 °C. The surface defects could be exposed after removing Na_2SO_4 by washing the sample in water.

The unique crystal defects induce an increase of surface area and the fairly large, porous nature of the chemically switched β-$Na_{0.33}V_2O_5$ as compared to the sol−gel-synthesized β-$Na_{0.33}V_2O_5$, which is also supported by the data from the BET surface area measurements (Figure 3c,d). The surface area of the chemically switched β-$Na_{0.33}V_2O_5$ is higher, whereas the average pore size decreases. Thus, the average pore size and surface area of the composite particles largely depend on the synthetic process because chemically switched β-$Na_{0.33}V_2O_5$ has the largest surface area and the highest number of pores. This can contribute to a shortened diffusion path of Li^+ ions and offer more active sites for electrochemical reactions as well as being a capacious container for electrolyte penetration into internal phases and a rigid scaffold to release the negative volumetric force from extraction and insertion process of lithium ions.

DOI: 10.1021/acsami.5b01260
ACS Appl. Mater. Interfaces 2015, 7, 7025−7032

3.2. Electrochemical Characterizations of the Samples. Cyclic voltammograms (CV) of β-$Na_{0.33}V_2O_5$ recorded at a scan rate of 0.1 mV s^{-1} are shown in Figure 4a. Well-defined

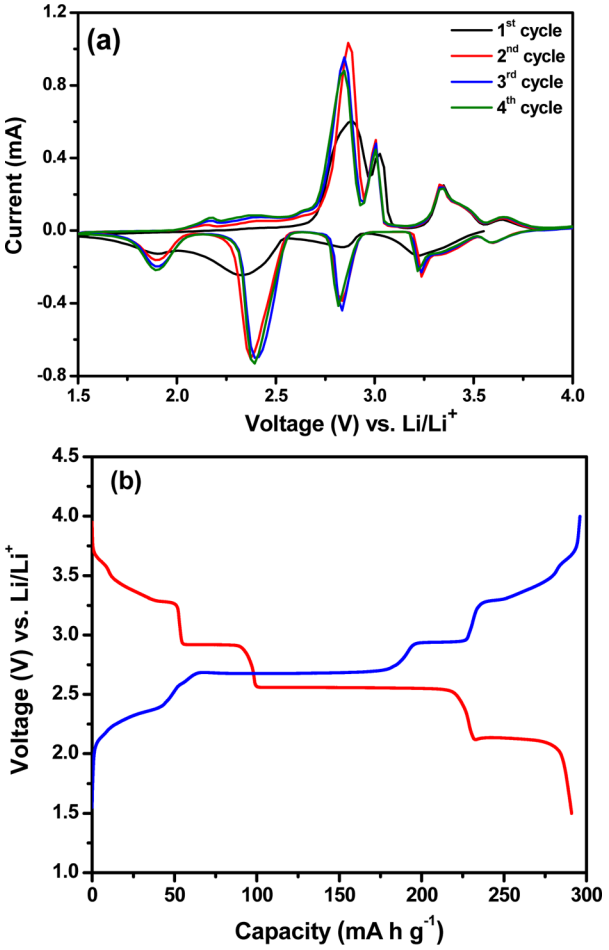

Figure 4. (a) CV of β-$Na_{0.33}V_2O_5$ at a scan rate of 0.1 mV s^{-1}. (b) Charge–discharge curve of β-$Na_{0.33}V_2O_5$ at a current density of 0.1 mA cm^{-2}.

oxidation/reduction peaks were observed in the CV curves. The cathodic peaks observed at 3.24, 2.82, 2.38, and 1.88 V belong to the multiple-step intercalation of lithium ions into the β-$Na_{0.33}V_2O_5$ phase. Similarly, deintercalation of lithium ions from the β-$Na_{0.33}V_2O_5$ phase was identified by anodic peaks at 2.17, 2.85, 3.02, and 3.34 V.[23,25] Charge–discharge curves of β-$Na_{0.33}V_2O_5$ recorded at a current density of 0.1 mA cm^{-2} are shown in Figure 4b. The four distinct voltage steps were observed at ~3.3, ~2.9, ~2.5, and ~2.1 V during the Li insertion into the β-$Na_{0.33}V_2O_5$ phase, which is consistent with the CV results. The first three voltage profiles located at 3.3, 2.9, and 2.5 V were assigned to the Li ion occupancy of the β-$Na_{0.33}V_2O_5$ structure's particular empty sites, M_3, M_2, and M_1, respectively (Figure 2b).[4] The Na ions were initially located at the M_1 sites of the β-$Na_{0.33}V_2O_5$ structure. During the discharging of the cell, when the voltage was 3.3 V, the Li ions began to occupy the M_3 sites of the β-$Na_{0.33}V_2O_5$ structure when $0 < x \leq 0.33$. The second voltage step at 2.9 V was assigned to the half-occupancy by the Li ions of the M_2 sites when $0.33 < x \leq 0.66$.[25] And finally, the large voltage plateaus at 2.5 V was assigned to the filling of the remaining M_1, M_2, and M_3 sites by the Li ions when $0.66 < x \leq 1.67$.[25] Such Li ion distribution to the M sites was reported to be thermodynamically and kinetically more favorable by minimizing the ion–ion repulsive Coulombic interactions during Li insertion into the β-$Na_{0.33}V_2O_5$ structure.[4] During Li insertion into β-$Na_{0.33}V_2O_5$, the Na ions of its structure were reported to be very stable even over a higher temperature range (100–450 °C).[6] As a result, the degree of Li insertion into the β-$Na_{0.33}V_2O_5$ structure is 1.67, but the total number of intercalated ions in the structure is 2 (= 0.33Na + 1.67Li).

To confirm the electrochemical extraction of Na from the β-$Na_{0.33}V_2O_5$ structure, the cell was charged first to 4.0 V (see Figure 5a). The charge voltage curve was observed at ~3.3 V,

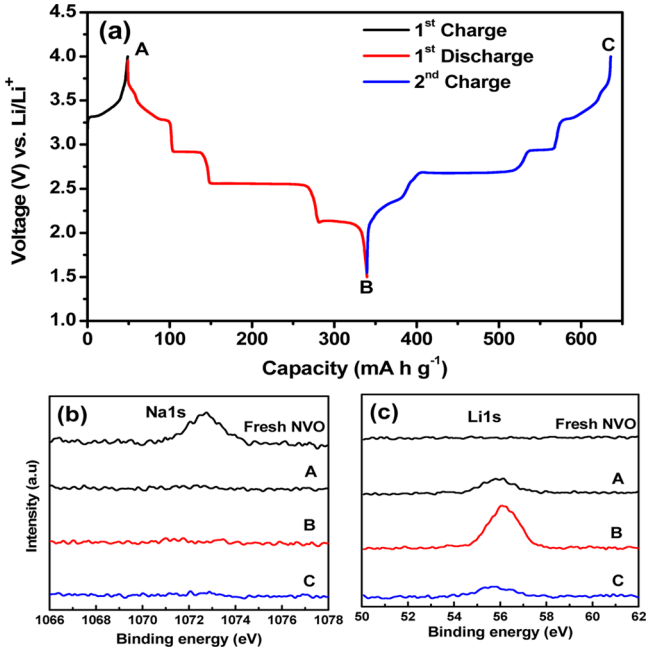

Figure 5. (a) Galvanostatic charge–discharge curve of β-$Na_{0.33}V_2O_5$ (NVO) (point labeled A is after first charge, B is after first discharge, and C is after second charge). Ex situ XPS of (b) Na 1s and (c) Li 1s.

and its capacity (47 mA h g^{-1}) corresponds well to the 0.33 Na per unit formula. The following discharge was performed to observe Li insertion into the structure. However, to eliminate the possibility of Na reinsertion into the structure, the Na-extracted electrode was collected after charging the cell and washed in DEC. This electrode was placed in the fresh coin cell with a Li metal anode and a 1 M $LiPF_6$ in EC:DEC electrolyte, which was discharged first to 1.5 V, as shown in Figure 5a. In addition to the reported three voltage steps at ~3.3, ~2.9, and ~2.5 V, a fourth voltage plateau was observed at 2.1 V when the cell was discharged to 1.5 V.

From these results, it can be expected that the Na ions are extracted from β-$Na_{0.33}V_2O_5$ during the charge process and that more Li ions are inserted into its structure during the discharge process, which results in the capacity increase after five cycles. Hence, the voltage step at 2.1 V can be related to the substitution of Na ions by Li ions in the β-$Na_{0.33}V_2O_5$ structure. So, the five well-defined Li insertion processes (the ~3.3 V sloped curve and the 2.9, 2.5, and 2.1 V potential plateaus) are connected with the Li content ranges of $0 < x \leq 0.33$, $0.33 < x \leq 0.66$, $0.66 < x \leq 1.67$, and $1.67 < x \leq 2.0$, respectively. This is in good accordance with the previous result that β-$Li_xV_2O_5$ was

DOI: 10.1021/acsami.5b01260
ACS Appl. Mater. Interfaces 2015, 7, 7025–7032

kept throughout a rather large voltage range of 1.5−4.5 V cutoff.[26−28]

The ex situ X-ray photoelectron spectroscopy (XPS) and energy-dispersive X-ray spectroscopy (EDX) measurements of Figures 5b,c and S3 clearly demonstrate Na-ion extraction and Li-ion insertion during the charge−discharge process. These results were consistent with the XPS and EDX measurements collected from the fresh electrode of β-$Na_{0.33}V_2O_5$, the first-charge electrode (charged to 4.0 V, position A), the first-discharge electrode (discharged to 1.5 V, position B), and the second-charge electrode (charged to 4.0 V again, position C). The β-$Na_{0.33}V_2O_5$ electrodes were carefully disassembled and washed by DEC and then investigated by XPS and SEM−EDX. Figure 5b,c shows the high-resolution XPS core-level spectra of Na 1s and Li 1s. After the first charge, the signal of Na 1s disappears and does not appear again. This indicates that the Na ion is extracted during the first charge and that the Li ion fills in the vacancy of the Na ion during discharge (position B). The height of the Li 1s peak is the same at positions A and C and that is the influence of lithium salt, which was placed on the surface of the electrode. The signal of Li 1s at position B of discharged β-$Na_{0.33}V_2O_5$ is much greater because of the insertion of Li ions into M sites (Figure 5c). The amount of Na content in the EDX of the charged β-$Na_{0.33}V_2O_5$ electrode was significantly lower compared with that of the fresh electrode, as shown in Figure 4d, which corresponds with the XPS result. Na is not found in β-$Na_{0.33}V_2O_5$ particles at positions A, B, and C by sodium SEM-mapping (Figure S4). Also, ex situ XRD patterns display the structure change with the extraction of Na ion and insertion of Li ion (Figure 6). β-

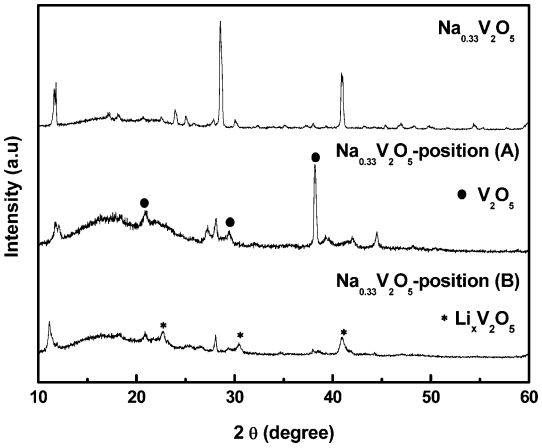

Figure 6. Ex situ XRD patterns of (A) fresh, charged and (B) discharged β-$Na_{0.33}V_2O_5$ electrodes.

$Na_{0.33}V_2O_5$ is transformed as V_2O_5 by the extraction of Na ions at position A. The XRD pattern of the recharged electrode (position C) shows $Li_xV_2O_5$ monoclinic structures with the insertion of lithium ions.

The chemically switched β-$Na_{0.33}V_2O_5$ showed in Figure 7 that the specific capacity of 284 mA h g^{-1} (after 1st discharge to 1.5 V) was increased to 295 mA h g^{-1} (after 10th discharge), which corresponds to $x \approx 2.0$ in $Li_x\beta$-$Na_{0.33}V_2O_5$. Impedance spectra for β-$Na_{0.33}V_2O_5$ at the 1st and 10th cycles are shown in Figure S4a. All three curves show a semicircle in the high-frequency region and an inclined line in the low-frequency region. The semicircle is assigned to the formation of solid electrolyte interface (SEI) and creates impedance at the surface

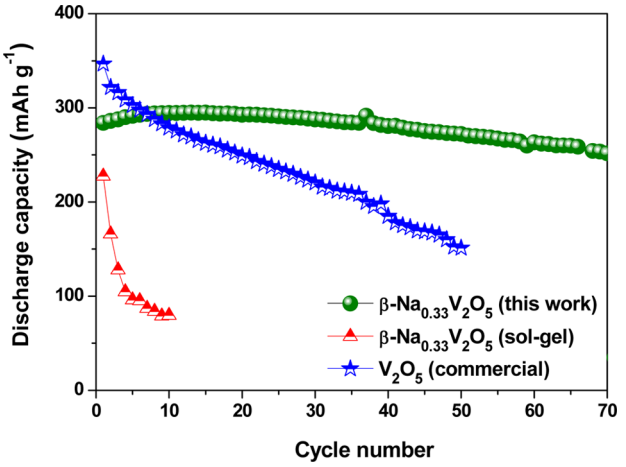

Figure 7. Cycling performance of β-$Na_{0.33}V_2O_5$ measured at the current rate of 0.1 mA cm^{-2} (cutoff = 4.0−1.5 V, room temperature).

of the electrode particles in contact with the organic electrolyte.[23,29] The increase in impedance observed in the first cycle is due to the development of the passivation film at the Li metal surface.[30] When increasing cycles, the high-frequency arc is decreased, which indicates the decrease in charge-transfer resistance. The lithium-ion diffusion coefficient (D) can be obtained either from the 45° portion of the line or by using eq 1, represented as[31,32]

$$D = \frac{R^2T^2}{2n^4F^4C^2\sigma^2} \quad (1)$$

where R is the gas constant, T is the temperature, n is the number of electrons per molecule during oxidization, F is the Faraday constant, C is the concentration of lithium ion, and σ is the Warburg factor. The Warburg factor σ can be obtained from eq 2, represented as

$$Z'' = \frac{\sigma\omega}{2} \quad (2)$$

Figure S4b shows the relationship between Z'' and the square root of frequency ($\omega^{-1/2}$) in the low-frequency region for β-$Na_{0.33}V_2O_5$ electrodes. The calculated lithium-ion diffusion coefficient for a fresh electrode is 1.3×10^{-15} m^2 s^{-1}, which increased to 4.1×10^{-15} m^2 s^{-1} for a cycled electrode. The capacity and voltage plateaus observed in the discharge process are very reversible during the charge process (Figure S5). Because the maximum number of Li ions that can be inserted into β-$Na_{0.33}V_2O_5$ is $x = 1.67$, it could be expected that the extra number of $x = 0.33$ correlates to the Li ions replacing the Na ions located at the M_1 sites. This was also observed in the recent electrochemical study of β-$Na_{0.33}V_2O_5$ nanorods,[22] where more than 1.6 Li intercalated into its nanorod structure was observed while extracting Na from the structure when the cell was discharged to 1.5 V. The comparative charge−discharge profile of chemically switched β-$Na_{0.33}V_2O_5$ with commercial V_2O_5 is shown in Figure S5. The electrochemical reaction is fully reversible where $0 \le x \le 1.5$ in general β-$Na_{0.33}V_2O_5$, prepared by the reported synthesis process.[18−20] However, for $x > 1.5$ the electrochemical reaction is no longer reversible when is discharged to below 2.2 V, which is the major reason for poor cycle stability (Figure 7). Electrochemically ion-exchanged $Li_xV_2O_5$ displays stable cycle performance up to 70 cycles, even deeply discharged to 1.5 V (Figure 7), because

DOI: 10.1021/acsami.5b01260
ACS Appl. Mater. Interfaces 2015, 7, 7025−7032

the efficient crystal structure and internal pores formed by crystal defects helps fast ion transfer with prevention of crystal collapse. $Li_xV_2O_5$ retains 89% capacity after 70 cycles with 99% Coulombic efficiency. However, the slight capacity fading observed is due to the slow lithium-ion diffusion for intercalation/deintercalation.[23,28]

To the best of our knowledge, this is the first work that reports Na ion extraction from β-$Na_{0.33}V_2O_5$ without irreversible structural change and further reversible Li-ion intercalation into its structure in the range of $0 \leq x \leq 2$. The chemical switch of $NaVS_2$ being heat-treated in air is a typical method to synthesize a high-quality sodium vanadium bronze, β-$Na_{0.33}V_2O_5$, with enhanced crystallinity. The 600 °C calcined sample showed high crystallinity with the formation of a high-temperature monoclinic β-$Na_{0.33}V_2O_5$ phase. The stable electrochemical performance of the sample is due to its highly crystalline nature. High-temperature annealing can improve the conductivity that is beneficial for facile electron transportation.[33−35] In addition, chemically switched β-$Na_{0.33}V_2O_5$ showed a porous nature and an increase in surface area (151.13 $m^2\ g^{-1}$) compared to the sol−gel-synthesized β-$Na_{0.33}V_2O_5$. The porous structure formed on the surface of the β-$Na_{0.33}V_2O_5$ phase and the unique crystal structure compared with that reported for β-$Na_{0.33}V_2O_5$ could stabilize the abrupt structural transformation during Li intercalation when cycling, which can be expected for the β-$Na_{0.33}V_2O_5$ phase reversibility.[23,24,28] The cell parameters of β-$Na_{0.33}V_2O_5$ prepared by chemical switch are different than those reported for typical β-$Na_{0.33}V_2O_5$, and the *b* axis is shorter, which is beneficial to ion diffusion and prevention of structure collapse.[24] Moreover, the high porosity of chemically switched β-$Na_{0.33}V_2O_5$ plays an important role to achieve high capacity, where $x \leq 2$ with deep discharges to 1.5 V, without structure collapse.[23]

4. CONCLUSIONS

The highly crystalline β-$Na_{0.33}V_2O_5$ was created via a new method of chemical switch, transforming the $NaVS_2$ sulfide by heat-treatment in atmospheric air. The chemically switched β-$Na_{0.33}V_2O_5$ showed rod-shaped particles that were 7−15 μm long and 1−3 μm wide. Also, β-$Na_{0.33}V_2O_5$ has a unique crystal structure with a short *b*-axis cell parameter and crystal defects, allowing high porosity and fast ion diffusion in the internal phase. β-$Na_{0.33}V_2O_5$ is converted into $Li_xV_2O_5$ by electrochemical ion exchange and enables deep discharge to 1.5 V to achieve high capacity. The ion-exchanged $Li_xV_2O_5$ delivered a high capacity of 285 mA h g^{-1} and showed stable cycle performance at 0.1 mA cm^{-2} in a voltage range of 1.5−4 V. This electrochemical process corresponds to a reversible insertion/extraction of two Li ($0 \leq x \leq 2$) by extracting Na from the β-$Na_{0.33}V_2O_5$ structure, although the reported β-$Na_{0.33}V_2O_5$ is possible up to $x = 1.67$ with $Li_x\beta$-$Na_{0.33}V_2O_5$. In addition, ex situ XPS, SEM−EDX, and ex situ XRD results supported the extraction of Na from the β-$Na_{0.33}V_2O_5$ structure. The large capacity of this sample is quite attractive in terms of increased energy density for Li-ion batteries. The β-$Na_{0.33}V_2O_5$ microsized particle prepared by chemical switch shows good structural reversibility when $0 \leq x \leq 2$, which has not been reported in any other literature.

■ ASSOCIATED CONTENT

Supporting Information

Additional XRD pattern, SEM images, SEM−EDX mapping, impedance spectra of β-$Na_{0.33}V_2O_5$ electrodes, and electrochemical performance for the $NaVS_2$ and heat-treated $NaVS_2$ samples. This material is available free of charge via the Internet at http://pubs.acs.org/.

■ AUTHOR INFORMATION

Corresponding Authors

*E-mail: junghyun.kim@gm.com.
*E-mail: ykim@unist.ac.kr.

Notes

The authors declare no competing financial interest.

■ ACKNOWLEDGMENTS

The work performed at Ulsan National Institute of Science and Technology was financially supported by National Research Foundation of Korea (NRF-2014R1A2A1A11052110). Part of the Microscopy research is supported by Oak Ridge National Laboratory's Shared Research Equipment (SHaRE) User Facility that is sponsored by the Office of Basic Energy Sciences, United States Department of Energy.

■ REFERENCES

(1) Whittingham, M. S. The Role of Ternary Phases in Cathode Reactions. *J. Electrochem. Soc.* **1976**, *123*, 315−320.
(2) Delmas, C.; Brèthes, S.; Ménétrier, M. ω-$Li_xV_2O_5$ — a New Electrode Material for Rechargeable Lithium Batteries. *J. Power Sources* **1991**, *34*, 113−118.
(3) Cartier, C.; Tranchant, a.; Verdaguer, M.; Messina, R.; Dexpert, H. X-ray diffraction and X-ray absorption studies of the structural modifications induced by electrochemical lithium intercalation into V_2O_5. *Electrochim. Acta* **1990**, *35*, 889−898.
(4) Cocciantelli, J. M.; Doumerc, J. P.; Pouchard, M.; Broussely, M.; Labat, J. Crystal chemistry of electrochemically inserted $LixV_2O_5$. *J. Power Sources* **1991**, *34*, 103−111.
(5) Zhai, T.; Liu, H.; Li, H.; Fang, X.; Liao, M.; Li, L.; Zhou, H.; Koide, Y.; Bando, Y.; Golberg, D. Centimeter-long V_2O_5 nanowires: From Synthesis to Field-Emission, Electrochemical, Electrical Transport, and Photoconductive Properties. *Adv. Mater.* **2010**, *22*, 2547−2552.
(6) Mai, L.; Xu, L.; Han, C.; Xu, X.; Luo, Y.; Zhao, S.; Zhao, Y. Electrospun Ultralong Hierarchical Vanadium Oxide Nanowires with High Performance for Lithium Ion Batteries. *Nano Lett.* **2010**, *10*, 4750−4755.
(7) Baddour-Hadjean, R.; Marzouk, a.; Pereira-Ramos, J. P. Structural modifications of $Li_xV_2O_5$ in a composite cathode ($0 \leq x < 2$) investigated by Raman microspectrometry. *J. Raman Spectrosc.* **2012**, *43*, 153−160.
(8) Asl, N. M.; Kim, J.-H.; Lee, W. C.; Liu, Z.; Lu, P.; Kim, Y. A new chemical route for the synthesis of β'-$Li_xV_2O_5$ for use as a high performance cathode. *Electrochim. Acta* **2013**, *105*, 403−411.
(9) Wang, Y.; Takahashi, K.; Lee, K.; Cao, G. Nanostructured Vanadium Oxide Electrodes for Enhanced Lithium-Ion Intercalation. *Adv. Funct. Mater.* **2006**, *16*, 1133−1144.
(10) Liu, D.; Liu, Y.; Garcia, B. B.; Zhang, Q.; Pan, A.; Jeong, Y.-H.; Cao, G. V_2O_5 xerogel electrodes with much enhanced lithium-ion intercalation properties with N_2 annealing. *J. Mater. Chem.* **2009**, *19*, 8789−8795.
(11) Zhang, X.; Wang, K.; Wei, X.; Chen, J. Carbon-Coated V_2O_5 Nanocrystals as High Performance Cathode Material for Lithium Ion Batteries. *Chem. Mater.* **2011**, *23*, 5290−5292.
(12) Su, D.; Wang, G.; Accepted, J. Single Crystalline Bilayered V_2O_5 Nanobelts for High Capacity Sodium-Ion Batteries. *ACS Nano* **2013**, *12*, 11218−11226.
(13) Gödickemeier, M. Engineering of Solid Oxide Fuel Cells with Ceria-Based Electrolytes. *J. Electrochem. Soc.* **1998**, *145*, 414−421.
(14) Xu, Y.; Han, X.; Zheng, L.; Yan, W.; Xie, Y. Pillar effect on Cyclability Enhancement for Aqueous Lithium ion batteries: a New

DOI: 10.1021/acsami.5b01260
ACS Appl. Mater. Interfaces 2015, 7, 7025−7032

Material of β-vanadium bronze $M_{0.33}V_2O_5$ (M = Ag, Na) nanowires. *J. Mater. Chem.* **2011**, *21*, 14466−14472.
(15) Raistrick, I. D. Lithium Insertion Reactions in Tungsten and Vanadium Bronzes. *Solid State Ionics* **1983**, *10*, 425−430.
(16) Raistrick, I. D. Lithium insertion reactions in oxide bronzes. *Rev. Chim. Miner.* **1984**, *21*, 456−467.
(17) Rabia, K.; Pashkin, a.; Frank, S.; Obermeier, G.; Horn, S.; Hanfland, M.; Kuntscher, C. A High-pressure XRD study of β-$Na_{0.33}V_2O_5$. *High Pressure Res.* **2009**, *29*, 504−508.
(18) Pereiraramos, J.; Messina, R.; Znaidi, L.; Baffier, N. Electrochemical lithium intercalation in $Na_{0.33}V_2O_5$ Bronze prepared by sol-gel processes. *Solid State Ionics* **1988**, *28−30*, 886−894.
(19) Bach, S. A. Thermodynamic and Kinetic Study of Electrochemical Lithium Intercalation in $Na_{0.33}V_2O_5$ Bronze Prepared by a Sol-Gel Process. *J. Electrochem. Soc.* **1990**, *137*, 1042−1048.
(20) Kim, Y.; Goodenough, J. B. Reinvestigation of $Li_{1-x}Ti_yV_{1-y}S_2$ Electrodes in Suitable Electrolyte: Highly Improved Electrochemical Properties. *Electrochem. Solid-State Lett.* **2009**, *12*, A73−A75.
(21) Khoo, E.; Wang, J.; Ma, J.; Lee, P. S. Electrochemical energy storage in a β-$Na_{0.33}V_2O_5$ nanobelt network and its application for supercapacitors. *J. Mater. Chem.* **2010**, *20*, 8368−8374.
(22) Liu, H.; Wang, Y.; Li, L.; Wang, K.; Hosono, E.; Zhou, H. Facile synthesis of NaV_6O_{15} nanorods and its electrochemical behavior as cathode material in rechargeable lithium batteries. *J. Mater. Chem.* **2009**, *19*, 7885−7891.
(23) Liang, S.; Zhou, J.; Fang, G.; Zhang, C.; Wu, J.; Tang, Y.; Pan, A. Synthesis of Mesoporous β-$Na_{0.33}V_2O_5$ with Enhanced Electrochemical Performance for Lithium ion batteries. *Electrochim. Acta* **2014**, *130*, 119−126.
(24) Tang, Y.; Sun, D.; Wang, H.; Huang, X.; Zhang, H.; Liu, S.; Liu, Y. Synthesis and electrochemical properties of NaV_3O_8 nano flakes as high-performance cathode for Li-ion battery. *RSC Adv.* **2014**, *4*, 8328−8334.
(25) Li, W. D.; Xu, C. Y.; Pan, X. L.; Huang, Y. D.; Zhen, L. High Capacity and Enhanced Structural Reversibility of β-$Li_xV_2O_5$ Nanorods as the Lithium Battery Cathode. *J. Mater. Chem. A* **2013**, *1*, 5361−5369.
(26) O'Dwyer, C.; Lavayen, V.; Tanner, D. a.; Newcomb, S. B.; Benavente, E.; González, G.; Torres, C. M. S. Reduced Surfactant Uptake in Three Dimensional Assemblies of VO_x Nanotubes Improves Reversible Li^+ Intercalation and Charge Capacity. *Adv. Funct. Mater.* **2009**, *19*, 1736−1745.
(27) Jiang, J.; Wang, Z.; Chen, L. Structural and Electrochemical Studies on β-$Li_xV_2O_5$ as Cathode Material for Rechargeable Lithium Batteries. *J. Phys. Chem. C* **2007**, *111*, 10707−10711.
(28) Baddour-Hadjean, R.; Bach, S.; Emery, N.; Pereira-Ramos, J. P. The peculiar structural behaviour of β-$Na_{0.33}V_2O_5$ upon electrochemical lithium insertion. *J. Mater. Chem.* **2011**, *21*, 11296−11305.
(29) Needham, S. A.; Wang, G. X.; Konstantinov, K.; Tournayre, Y.; Lao, Z.; Liu, H. K. Electrochemical Performance of Co_3O_4−C Composite Anode Materials. *Electrochem. Solid-State Lett.* **2006**, *9*, A315−A319.
(30) Schweikert, N.; Hahn, H.; Indris, S. Cycling behaviour of Li/$Li_4Ti_5O_{12}$ cells studied by electrochemical impedance spectroscopy. *Phys. Chem. Chem. Phys.* **2011**, *13*, 6234−6240.
(31) Gao, F.; Tang, Z. Kinetic behavior of $LiFePO_4$/C cathode material for lithium-ion batteries. *Electrochim. Acta* **2008**, *53*, 5071−5075.
(32) Kim, J. K.; Manuel, J.; Chauhan, G. S.; Ahn, J. H.; Ryu, H. S. Ionic liquid-based gel polymer electrolyte for $LiMn_{0.4}Fe_{0.6}PO_4$ cathode prepared by electrospinning technique. *Electrochim. Acta* **2010**, *55*, 1366−1372.
(33) Huang, S.-Z.; Cai, Y.; Jin, J.; Li, Y.; Zheng, X.-F.; Wang, H.-E.; Wu, M.; Chen, L.-H.; Su, B.-L. Annealed vanadium oxide nanowires and nanotubes as high performance cathode materials for lithium ion batteries. *J. Mater. Chem. A* **2014**, *2*, 14099−14108.
(34) Doherty, C. M.; Caruso, R. A.; Smarsly, B. M.; Drummond, C. J. Colloidal Crystal Templating to Produce Hierarchically Porous $LiFePO_4$ Electrode Materials for High Power Lithium Ion Batteries. *Chem. Mater.* **2009**, *21*, 2895−2903.
(35) Liu, W. L.; Tu, J. P.; Qiao, Y. Q.; Zhou, J. P.; Shi, S. J.; Wang, X. L.; Gu, C. D. Optimized performances of core−shell structured $LiFePO_4$/C nanocomposite. *J. Power Sources* **2011**, *196*, 7728−7735.

DOI: 10.1021/acsami.5b01260
ACS Appl. Mater. Interfaces 2015, 7, 7025−7032